Shaping Magnetite Nanoparticles from First Principles

Hongsheng Liu and Cristiana Di Valentin*
Dipartimento di Scienza dei Materiali, Università di Milano-Bicocca, via Roberto Cozzi 55, I-20125 Milano, Italy

(Received 17 June 2019; revised manuscript received 12 September 2019; published 29 October 2019)

Iron oxide magnetic nanoparticles (NPs) are stimuli-responsive materials at the forefront of nanomedicine. Their realistic finite temperature simulations are a formidable challenge for first-principles methods. Here, we use density functional tight binding to open up the required time and length scales and obtain global minimum structures of Fe_3O_4 NPs of realistic size (1400 atoms, 2.5 nm) and of different shapes, which we then refine with hybrid density functional theory methods to accomplish proper electronic and magnetic properties, which have never been accurately described in simulations. On this basis, we develop a general empirical formula and prove its predictive power for the evaluation of the total magnetic moment of Fe_3O_4 NPs. By converting the total magnetic moment into the macroscopic saturation magnetization, we rationalize the experimentally observed dependence with shape. We also reveal interesting reconstruction mechanisms and unexpected patterns of charge ordering.

DOI: 10.1103/PhysRevLett.123.186101

Magnetite (Fe_3O_4) nanoparticles (NPs) are top-class materials for biomedical applications because of their excellent soft magnetism (high saturation magnetization and low coercive force), good biocompatibility, and low cytotoxicity [1,2]. They constitute the new generation contrast agents for magnetic resonance imaging (MRI) and are effective carriers for targeted drug delivery, heating agents in magnetic hyperthermia, adsorbents for magnetic bioseparation, and biosensors [3–9].

Monodisperse Fe_3O_4 NPs with sizes variable from 3 to 22 nm in diameter have been successfully prepared [10–14] with different shapes, including cubes, octahedra, rhombic dodecahedra, truncated octahedra, and spheres [15–24]. Magnetite NPs are found to be superparamagnetic above the blocking temperature and ferrimagnetic below it [11,12,14–16,23,24]. Furthermore, tunneling microscopy shows that below the Verwey temperature magnetite NPs are semiconductors with a small band gap from 0.14 to 0.30 eV [25,26].

Despite the relevance of magnetite NPs in nanobiotechnology, we observe a severe lack of a theoretical framework, which could assist in the interpretation of experimental findings at an atomic scale and guide further experiments. For instance, only recently the $\sqrt{2} \times \sqrt{2}$ reconstruction of the clean $Fe_3O_4(001)$ single crystal surface was revealed by Bliem *et al.* [27] through a combined experimental and theoretical study. This begs the next question: what kind of reconstructions may arise in a nanoconfined magnetite particle?

Unfortunately, magnetite is a complex material to be described accurately by theoretical methods. We have shown that, to catch proper structural, electronic, and magnetic properties of even the most simple bulk and flat surface systems, high-level quantum mechanical (QM) techniques, beyond standard density functional theory (DFT), are required [28,29]. Up to now, magnetite nanoparticles have only been addressed by force-field methods to study their interaction with surfactants [30–33]. However, these types of simulations have some intrinsic limitations, since they cannot provide any information on the electronic and magnetic structure, cannot handle bond breaking and bond formation, and have limited transferability.

With the present Letter, we make a major breakthrough in the theoretical modeling of magnetite nanosystems. First, we solve the critical problem of the correct assignment of the total magnetic moment (m_{tot}) to magnetite model nanostructures and provide the community with a validated general empirical formula for its *a priori* evaluation. From that we derive the saturation magnetization (M_S) of an ideal macroscopic sample of all identical NPs for comparison with experiments. Then, by combining density functional tight binding (DFTB) [34] and hybrid DFT methods [35], we accomplish the quantum mechanical simulation of Fe_3O_4 NPs of realistic size in both cubic (1466 atoms, edge length of 2.3 nm) and spherical (1006 atoms, diameter of 2.5 nm) shapes. Global minimum atomic-scale structures of the NPs are obtained by high-temperature annealing simulations with the Hubbard corrected DFTB (DFTB+U) method, followed by full atomic relaxation with hybrid DFT. Interesting reconstruction mechanisms and unexpected patterns of charge ordering are revealed. A rational basis for the larger experimentally observed M_S of nanocubes with respect to nanospheres is also derived from our results.

This Letter fills the existing gap in the quantum chemical description of magnetite NPs of realistic size and paves the way for further theoretical studies for the benefit of both the computational and experimental communities.

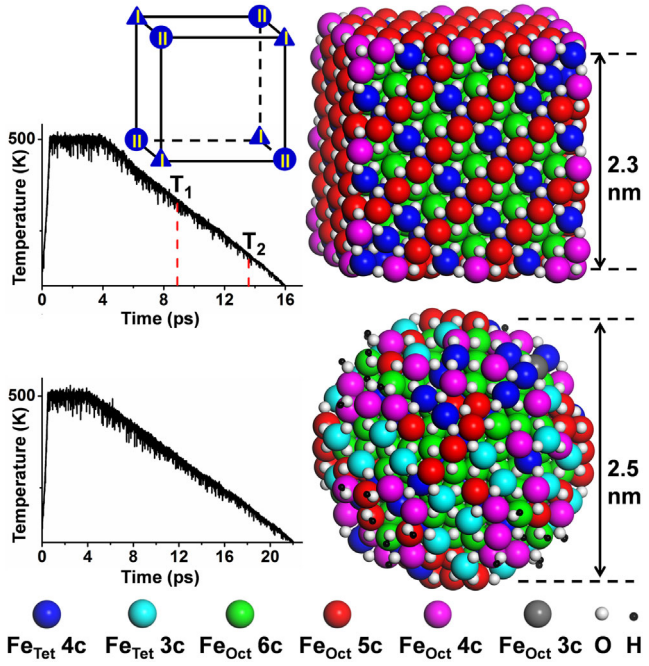

FIG. 1. Simulated annealing temperature profiles and global minimum structures of the magnetite nanocube (up) and nanosphere (down). The color coding of atoms is given in the legend at the bottom. Labels 3c–6c indicate the actual coordination number of the corresponding ions. (Inset) Shows the two types of corners.

Here, molecular dynamics (MD) simulations were performed with self-consistent charge DFTB method, as implemented in the DFTB+ package [36], to search for the global minimum structure of Fe_3O_4 NPs. Then, hybrid functional calculations (the Heyd-Scuseria-Ernzerhof (HSE) screened hybrid functional [35]) were carried out using the CRYSTAL17 package [37,38] to get the final optimized structures and electronic and magnetic properties of the nanoparticles. Further computational details can be found in the Supplemental Material [39].

Considering the frequent observation of cubic Fe_3O_4 NPs enclosed by six (001) facets in experiments [15–17], we carved from the bulk a magnetite nanocube ($Fe_{602}O_{864}$) of 1466 atoms with edge length of 2.3 nm in a way that the lowest coordination of Fe and O atoms is four- and twofold, respectively. We define two kinds of Fe ions in the NP, Fe_{Tet} and Fe_{Oct}, depending on the occupied bulk lattice site (tetrahedral and octahedral), even when they become undercoordinated at the surface. The nanocube is in the T_d symmetry and presents two types of corner sites (see Fig. 1): (a) four corners expose an Fe_{Tet} ion at the apex (type I) and (b) four corners expose an O atom at the apex (type II).

The first challenge one must face to perform the QM simulation of a magnetite NP is the definition of its optimal total magnetic moment (m_{tot}), as discussed in detail in the Supplemental Material [39]. To overcome this challenge, we propose (and validate in this work below) an empirical formula for m_{tot},

$$m_{tot} = 5 \times [N(Fe^{3+}_{Oct}) - N(Fe^{3+}_{Tet})] + 4 \times [N(Fe^{2+}_{Oct}) - N(Fe^{2+}_{Tet})], \quad (1)$$

where Fe^{3+}_{Oct} and Fe^{2+}_{Oct} are Fe^{3+} and Fe^{2+} ions at octahedral sites, Fe^{3+}_{Tet} and Fe^{2+}_{Tet} are Fe^{3+} and Fe^{2+} ions at tetrahedral sites, and N is the number of the corresponding ions. This formula can be interpreted by means of the crystal field theory and the d orbitals occupation of different Fe ions in bulk magnetite, in line with what was previously observed by hybrid DFT calculations [28]: for Fe^{3+}_{Oct} and Fe^{3+}_{Tet}, the high-spin $3d^5$ electron configuration gives an atomic magnetic moment of $+5$ and -5 μ_B, respectively; for Fe^{2+}_{Oct} and Fe^{2+}_{Tet}, the high-spin $3d^6$ electron configuration gives $+4$ μ_B and -4 μ_B, respectively. For the nanocube, since all Fe_{Tet} ions are assumed to be charged 3+ and O ions -2, $N(Fe^{3+}_{Oct})$ and $N(Fe^{2+}_{Oct})$ can be easily calculated. This formula works perfectly for magnetite bulk and (001) surfaces and gives $m_{tot} = 1232$ μ_B for the carved nanocube.

The nanocube global minimum structure was searched by MD simulations with the DFTB + U method that simulates a temperature annealing process up to 500 K (Fig. 1). We recently proved that DFTB + U, with our newly proposed parametrization of the Fe—O interactions, is very efficient and satisfactorily reliable for the description of bulk and surface magnetite [45]. With this computationally cheaper method, one can perform simulations for systems of a thousand atoms or more on timescales of tenths of picoseconds, which is well beyond what is currently accessible with first-principles MD simulations. During the annealing, the four type-I corners underwent reconstructions at time T_1 and T_2, as shown in Fig. 1. Compared with the structure before annealing, the reconstructed nanocube is about 14 meV per atom lower in energy. To clarify the reconstruction mechanism, the top and side views of one of the three (001) facets that meet at the type-I corner are displayed in Fig. 2. The process consists of the transfer of 3 six-coordinated Fe_{Oct} ions around the corner (green large spheres) to 3 four-coordinated Fe_{Tet} ions (marked as 1, 2, and 3). The top and side views of the other two (001) facets that meet at this corner are exactly the same as the one shown in Fig. 2, but with Fe_{Tet} 2 or 3 in the place of Fe_{Tet} 1, respectively. This reconstruction presents some analogies to that proposed for single crystal (001) surfaces [27]. However, in that case, every two Fe vacancies at octahedral sites in the subsurface layer are replaced only by one additional tetrahedral Fe, leading to an unbalanced Fe:O stoichiometry.

The DFTB + U optimized reconstructed nanocube structure was confirmed by full atomic relaxation with the more sophisticated HSE hybrid functional. For nanocubes of larger size, we expect the same reconstruction at the corners, since this atomic rearrangement only involves few atoms around corners.

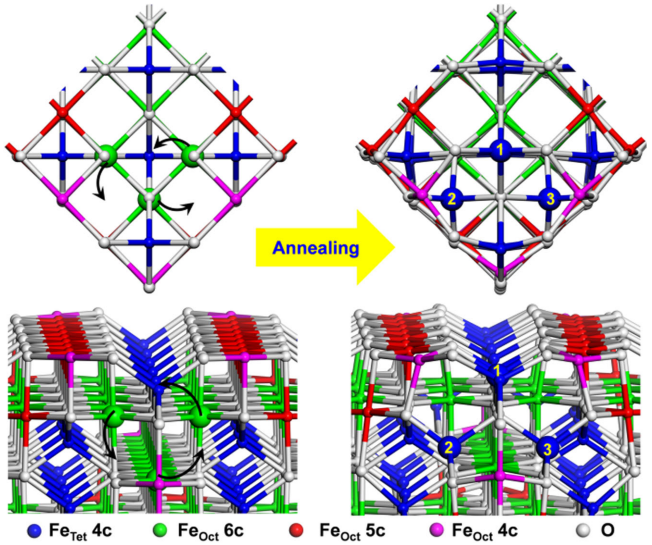

FIG. 2. Top and side views of one of the three (001) facets that meet at the type-I corners of the nanocube, before and after annealing. The color coding of atoms is given in the legend at the bottom. Labels 3c–6c indicate the actual coordination number of the corresponding ions. The black arrows indicate the motion of atoms during the annealing process.

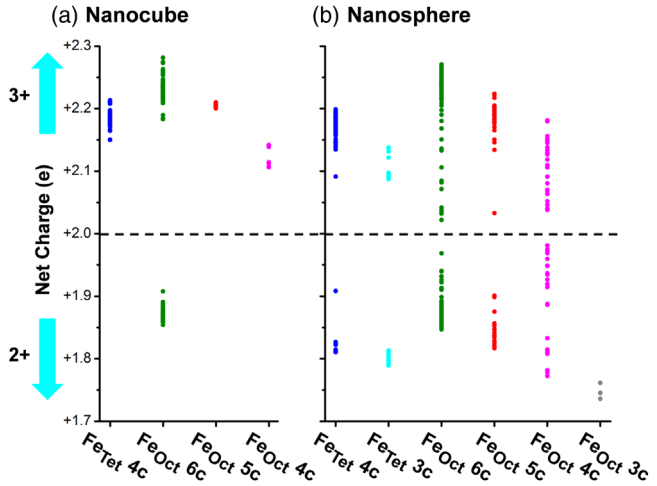

FIG. 3. The net charge distribution for the Fe ions with different coordination at tetrahedral and octahedral sites in the optimized Fe_3O_4 (a) nanocube and (b) nanosphere with HSE functional after simulated annealing. Labels 3c–6c indicate the actual coordination number of the corresponding ions.

Note that, after reconstruction, the total number of Fe_{Tet} and Fe_{Oct} has changed (see Table S1 in the Supplemental Material [39]). If we apply formula (1), we get an m_{tot} of 1112 μ_B for the reconstructed nanocube vs 1232 μ_B for the unreconstructed one. In order to validate the equation, we performed a series of HSE calculations, where we fully relaxed the nanocube atomic positions while varying m_{tot} (see Fig. S1 in the Supplemental Material [39]). The minimum total energy is registered for $m_{tot} = 1112\ \mu_B$, in perfect agreement with the output by Eq. (1). Therefore, we conclude that this formula is rather general since it works for different situations ranging from bulk to surface to nanocube. The reconstruction reduces the m_{tot} of the NP by about 10%.

Since in many biomedical applications magnetite NPs are spherical [30,46,47,48], we prepared another model of stoichiometric curved NPs $[(Fe_3O_4)_{136}(H_2O)_{18}]$ by carving a sphere of 2.5 nm diameter and including 18 dissociatively adsorbed water molecules to saturate the too-low-coordinated Fe and O ions. Different from what was observed for nanocubes, for spherical NPs the $N(Fe^{2+}_{Tet})$ term is not null (as discussed below) and must be obtained by DFT calculations. Therefore, we performed a series of full atomic relaxation calculations with the HSE06 functional at different m_{tot} values to determine the optimal $m_{tot}(600\ \mu_B)$, as shown in Fig. S2 in the Supplemental Material [39]. Using the Fe ions distribution in lowest energy configuration and formula (1), we get m_{tot} of 602 μ_B with a 0.3% error with respect to the HSE optimal value. Considering the complexity of the curved surface, this simple formula works more than satisfactorily.

During the annealing process, simulated with DFTB + U, large atomic rearrangements occur at the curved surface to reduce the number of low-coordinated Fe ions (see Table S1 in the Supplemental Material [39]), which involves the conversion of some six- and four-coordinated Fe_{Oct} ions into five-coordinated ones and, in parallel, the conversion of some three-coordinated Fe_{Tet} ions into four-coordinated ones. The resulting energy stabilization is of about 14 meV per atom. The annealed structure was then fully relaxed with the HSE functional (see Fig. 1). Similar atomic rearrangements are expected for larger spherical NPs. With the size increasing, the NP becomes more and more faceted and the percentage of low-coordinated cations decreases, as found in our previous work on TiO_2 NPs [49].

DFTB + U and HSE structures are compared by simulating the extended X-ray adsorption fine structure in real space (see Figs. S3 and S4 and detailed discussion in the Supplemental Material [39]). The satisfactory agreement confirms the suitability of DFTB + U for the description of structural properties of magnetite NPs and supports its use for thermal annealing simulations.

The charge ordering in magnetite is an interesting and challenging topic. Large efforts have been devoted to its understanding in the case of bulk during recent years [28,50–55], whereas, up to now, no information has been reported in the case of NPs. Hybrid functional calculations can provide precious information on charge distribution [28]. Here, we analyze Mulliken population charges, based on HSE calculations, to determine the Fe^{2+} and Fe^{3+} distribution. For the nanocube, we observe that all the Fe_{Tet} ions are 3+, whereas Fe_{Oct} are divided into two groups: Fe^{2+}_{Oct} and Fe^{3+}_{Oct}, as shown in Fig. 3(a). All the low-coordinated Fe_{Oct} ions (5c and 4c) on the NP surface are charged 3+. We show dissected views of the nanocube (Fig. 4, top) indicating

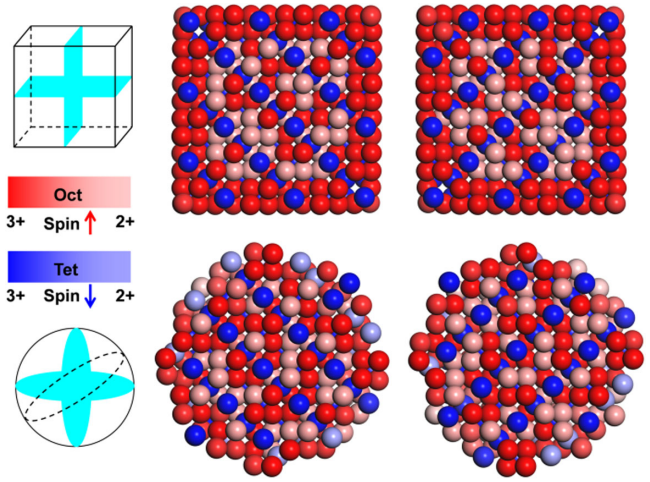

FIG. 4. Selected dissected views showing the charge and spin distribution in the magnetite nanocube and nanosphere optimized models by HSE calculations. Oxygen atoms are not shown.

an interesting core-shell structure with Fe^{3+} ions in the outer-shell layers and alternating Fe^{2+}/Fe^{3+} ions in the core.

Different from the nanocube, the charge distribution on Fe_{Oct} becomes blurred for the nanosphere [see Fig. 3(b)]. For discussion convenience, Fe ions with a net charge less than +2 are labeled as Fe^{2+} and those with net charge more than +2 are labeled as Fe^{3+}. Interestingly, Fe^{2+}_{Tet} ions, not present in bulk, surface, or cubic NP systems, arise on the nanosphere surface because they are mostly three coordinated and highly distorted (see light blue spheres in Fig. 4). Fe^{2+}_{Oct} ions are distributed both in the core and at the surface of the NP (see light red spheres in Fig. 4).

The atomic magnetic moments of Fe^{2+} and Fe^{3+} in the NPs (listed in Table I) are similar to those calculated for the bulk corresponding species [28], except for Fe^{2+}_{Tet}. The absolute value of the atomic magnetic moment of Fe^{2+}_{Tet} is similar to that of Fe^{2+}_{Oct}.

We may note that, similar to bulk, in both nanocube and nanosphere models, Fe_{Tet} ions always couple antiferromagnetically with Fe_{Oct} ions. Being the latter in excess, the NPs are ferrimagnetic (Fig. 4 and Table I).

TABLE I. Average atomic magnetic moments (m) of Fe ions at tetrahedral and octahedral sites, total magnetic moment (m_{tot}) and saturation magnetization (M_S) for the magnetite nanocube and nanosphere (HSE) models.

	Nanocube	Nanosphere
$m(Fe^{3+}_{Tet})$ (μ_B)	−4.21	−4.18
$m(Fe^{2+}_{Tet})$ (μ_B)	⋯	−3.70
$m(Fe^{3+}_{Oct})$ (μ_B)	4.27	4.20
$m(Fe^{2+}_{Oct})$ (μ_B)	3.75	3.78
m_{tot} (μ_B)	1112	600
M_S(emu/g)	130.9	105.3

As a further step in our analysis of the magnetic properties of magnetite nanoparticles, starting from the calculated optimal m_{tot} value for the model NPs, presented in the previous section and reported also in Table 1, it is possible to estimate the M_S value (per gram) for an ideal macroscopic sample of identical NPs. Such quantity can be compared with experimental measurements. For the nanocube, we obtain $M_S = 130.9$ emu/g, which is larger than that for the nanosphere (105.3 emu/g), in agreement with experimental observations [15]. This result can be rationalized by analyzing the number of Fe_{Oct} and Fe_{Tet} ions [$N(Fe_{Oct})$ and $N(Fe_{Tet})$] in the NP. Because Fe_{Oct} and Fe_{Tet} couple antiferromagnetically, the net magnetic moment is determined by the excess of Fe_{Oct}, i.e., the difference between $N(Fe_{Oct})$ and $N(Fe_{Tet})$. The ratio of $N(Fe_{Oct})/N(Fe_{Tet})$ in the nanocube (2.3) is larger than that in the nanosphere (2.0) (see Table S1 in the Supplemental Material [39]), which accounts for the larger m_{tot} and thus larger M_S of the nanocube. From this point of view, nanocubes are more desirable for biomedical applications. We must note that the calculated M_S values are larger than the experimental ones (54.0 emu/g for nanocubes with a size of 6.5 nm at 5 K [16] and about 35 emu/g for nanospheres with diameter of 5 nm at 20 K [24]). This is probably due to the antiphase boundary structural defects in the experimental NPs, which can largely reduce the magnetization [56]. In addition, the presence of nonmagnetic surfactants on the particle surface in experiments can also be a cause of magnetization reduction.

Both the nanocube and the nanosphere models possess larger M_S than bulk (96 emu/g), which suggests that the larger the surface-to-bulk ratio, the larger the M_S. Therefore, the M_S should decrease with the size increase. We calculated the M_S of nanocubes of different sizes through formula (1) and the results confirm this trend, as shown in Fig. S5 in the Supplemental Material [39].

To get further insight into the electronic properties of magnetite NPs, we also present total and projected density of states on the d states of different Fe ions (Fig. S6) with the HSE method. NPs of both shapes have semiconducting character, which agrees with the tunneling microscopy measurements [25,26]. The nanocube possesses very similar electronic structure to that of bulk [28] and of the (001) surface [29], with a band gap of 0.55 eV. The conductivity is dominated by electron hopping between fully coordinated Fe^{2+}_{Oct} and Fe^{3+}_{Oct} in the core of the nanocube [Fig. S6(b)], but not on the surface, because there only Fe^{3+} ions are present (see Fig. 4, top). For the nanosphere, new surface states arise below the Fermi level (see Figs. S6 and S7 in the Supplemental Material [39]). However, the band gap (0.53 eV) is similar to nanocubes. Electron hopping can take place both in the bulk and on the surface, thanks to the presence of $Fe^{2+}_{Oct}/Fe^{3+}_{Oct}$ and $Fe^{2+}_{Tet}/Fe^{3+}_{Tet}$ (see Fig. 4).

In summary, by adopting a set of proper methods, including a general empirical formula for the *a priori*

determination of the optimal total magnetic moment and the combination of DFTB and hybrid DFT, we have accomplished the QM simulation of cubic and spherical Fe_3O_4 NPs of realistic size (2.3–2.5 nm). The optimized atomic structures were obtained through simulated annealing at 500 K by MD with the DFTB method, followed by full atomic relaxation with hybrid DFT. From the m_{tot} of one NP model, we can derive the macroscopic M_S for an ideal sample of all identical NPs, to be compared with experimentally measured values.

Our results reveal the surface reconstruction mechanism that takes place at the four Fe-exposing corners of the nanocube and that reduces the m_{tot} of the NP. Large atomic rearrangements also occur at the curved surface of the nanosphere to reduce the number of exposed low-coordinated Fe ions. The nanocube exhibits an interesting core-shell structure with respect to the distribution of Fe^{2+} and Fe^{3+}, resulting in an insulating state in the shell and a semiconducting one in the core. In contrast, the appearance of Fe^{2+}_{Tet} on the surface of the nanosphere makes the electrons hopping between Fe^{2+}_{Tet} and Fe^{3+}_{Tet} on the surface possible. Cubic NPs possess larger M_S than spherical ones due to the larger ratio of $N(Fe_{Oct})/N(Fe_{Tet})$ and thus are more desirable for biomedical applications.

The approach of formula (1) for the *a priori* determination of the optimal total magnetic moment, based on the principles of the crystal field theory, is also expected to be applicable to other magnetic materials of the spinel group, such as $MnFe_2O_4$, $NiFe_2O_4$, $CoFe_2O_4$, and so on. Therefore, our Letter not only makes possible to achieve the correct description, at the first-principles level of theory, of Fe_3O_4 nanoparticles, but also paves the way for the modeling of nanostructures of other similar magnetic materials.

The authors are grateful to Annabella Selloni and Gotthard Seifert for fruitful discussions, and to Lorenzo Ferraro for his technical help. The project has received funding from the European Research Council (ERC) under the European Union's HORIZON2020 Research and Innovation Programme (ERC Grant Agreement No. 647020).

*cristiana.divalentin@unimib.it

[1] J. M. Perez, L. Josephson, T. O'Loughlin, D. Högemann, and R. Weissleder, Magnetic relaxation switches capable of sensing molecular interactions, Nat. Biotechnol. **20**, 816 (2002).

[2] J. Liu, Z. Sun, Y. Deng, Y. Zou, C. Li, X. Guo, L. Xiong, Y. Gao, F. Li, and D. Zhao, Highly water-dispersible biocompatible magnetite particles with low cytotoxicity stabilized by citrate groups, Angew. Chem., Int. Ed. Engl. **48**, 5875 (2009).

[3] W. Wu, Z. Wu, T. Yu, C. Jiang, and W. Kim, Recent progress on magnetic iron oxide nanoparticles: Synthesis, surface functional strategies and biomedical applications, Sci. Technol. Adv. Mater. **16**, 023501 (2015).

[4] Q. A. Pankhurst, N. T. K. Thanh, S. K. Jones, and J. Dobson, Progress in applications of magnetic nanoparticles in biomedicine, J. Phys. D **42**, 224001 (2009).

[5] A. K. Gupta and M. Gupta, Synthesis and surface engineering of iron oxide nanoparticles for biomedical applications, Biomaterials **26**, 3995 (2005).

[6] C. Sun, J. S. Lee, and M. Zhang, Magnetic nanoparticles in MR imaging and drug delivery, Adv. Drug Delivery Rev. **60**, 1252 (2008).

[7] Q. A. Pankhurst, J. Connolly, S. K. Jones, and J. Dobson, Applications of magnetic nanoparticles in biomedicine, J. Phys. D **36**, R167 (2003).

[8] S. Laurent, D. Forge, M. Port, A. Roch, C. Robic, L. V. Elst, and R. N. Muller, Magnetic iron oxide nanoparticles: Synthesis, stabilization, vectorization, physicochemical characterizations, and biological applications, Chem. Rev. **108**, 2064 (2008).

[9] M. Colombo, S. Carregal-Romero, M. F. Casula, L. Gutiérrez, M. P. Morales, I. B. Böhm, J. T. Heverhagen, D. Prosperi, and W. J. Parak, Biological applications of magnetic nanoparticles, Chem. Soc. Rev. **41**, 4306 (2012).

[10] S. Sun and H. Zeng, Size-controlled synthesis of magnetite nanoparticles, J. Am. Chem. Soc. **124**, 8204 (2002).

[11] Y. Hou, J. Yu, and S. Gao, Solvothermal reduction synthesis and characterization of superparamagnetic magnetite nanoparticles, J. Mater. Chem. **13**, 1983 (2003).

[12] S. Sun, H. Zeng, D. B. Robinson, S. Raoux, P. M. Rice, S. X. Wang, and G. Li, Monodisperse MFe_2O_4 (M = Fe, Co, Mn) nanoparticles, J. Am. Chem. Soc. **126**, 273 (2004).

[13] J. Park, K. An, Y. Hwang, J. Park, H. Noh, J. Kim, J. Park, N. Hwang, and T. Hyeon, Ultra-large-scale syntheses of monodisperse nanocrystals, Nat. Mater. **3**, 891 (2004).

[14] Y. Tian, B. Yu, X. Li, and K. Li, Facile solvothermal synthesis of monodisperse Fe_3O_4 nanocrystals with precise size control of one nanometre as potential MRI contrast agents, J. Mater. Chem. **21**, 2476 (2011).

[15] M. V. Kovalenko, M. I. Bodnarchuk, R. T. Lechner, G. Hesser, F. Schäffler, and W. Heiss, Fatty acid salts as stabilizers in size- and shape-controlled nanocrystal synthesis: The case of inverse spinel iron oxide, J. Am. Chem. Soc. **129**, 6352 (2007).

[16] H. Yang, T. Ogawa, D. Hasegawa, and M. Takahashi, Synthesis and magnetic properties of monodisperse magnetite nanocubes, J. Appl. Phys. **103**, 07D526 (2008).

[17] D. Kim, N. Lee, M. Park, B. H. Kim, K. An, and T. Hyeon, Synthesis of uniform ferrimagnetic magnetite nanocubes, J. Am. Chem. Soc. **131**, 454 (2009).

[18] L. Zhao and L. Duan, Uniform Fe_3O_4 octahedra with tunable edge length-synthesis by a facile polyol route and magnetic properties, Eur. J. Inorg. Chem. **2010**, 5635 (2010).

[19] L. Zhang, J. Wu, H. Liao, Y. Hou, and S. Gao, Octahedral Fe_3O_4 nanoparticles and their assembled structures, Chem. Commun. 4378 (2009) https://doi.org/10.1039/b906636e.

[20] X. Li, D. Liu, S. Song, X. Wang, X. Ge, and H. Zhang, Rhombic dodecahedral Fe_3O_4: Ionic liquid-modulated and

microwave-assisted synthesis and their magnetic properties, CrystEngComm **13**, 6017 (2011).
[21] X. Cheng, J. Jiang, D. Jiang, and Z. Zhao, Synthesis of rhombic dodecahedral Fe_3O_4 nanocrystals with exposed high-energy {110} facets and their peroxidase-like activity and lithium storage properties, J. Phys. Chem. C **118**, 12588 (2014).
[22] R. Zheng, H. Gu, B. Xu, K. K. Fung, X. Zhang, and S. P. Ringer, Self-assembly and self-orientation of truncated octahedral magnetite nanocrystals, Adv. Mater. **18**, 2418 (2006).
[23] L. Zhao, H. Zhang, Y. Xing, S. Song, S. Yu, W. Shi, X. Guo, J. Yang, Y. Lei, and F. Cao, Morphology-controlled synthesis of magnetites with nanoporous structures and excellent magnetic properties, Chem. Mater. **20**, 198 (2008).
[24] K. Woo, J. Hong, S. Choi, H. Lee, J. Ahn, C. S. Kim, and S. W. Lee, Easy synthesis and magnetic properties of iron oxide nanoparticles, Chem. Mater. **16**, 2814 (2004).
[25] A. Hevroni, M. Bapna, S. Piotrowski, S. A. Majetich, and G. Markovich, Tracking the Verwey transition in single magnetite nanocrystals by variable-temperature scanning tunneling microscopy, J. Phys. Chem. Lett. **7**, 1661 (2016).
[26] Q. Yu, Verwey transition in single magnetite nanoparticles, Phys. Rev. B **90**, 075122 (2014).
[27] R. Bliem, E. McDermott, P. Ferstl, M. Setvin, O. Gamba, J. Pavelec, M. A. Schneider, M. Schmid, U. Diebold, P. Blaha, L. Hammer, and G. S. Parkinson, Subsurface cation vacancy stabilization of the magnetite (001) surface, Science **346**, 1215 (2014).
[28] H. Liu and C. Di Valentin, Band gap in magnetite above Verwey temperature induced by symmetry breaking, J. Phys. Chem. C **121**, 25736 (2017).
[29] H. Liu and C. Di Valentin, Bulk-terminated or reconstructed $Fe_3O_4(001)$ surface: Water makes a difference, Nanoscale **10**, 11021 (2018).
[30] M. Patitsa, K. Karathanou, Z. Kanaki, L. Tzioga, N. Pippa, C. Demetzos, D. A. Verganelakis, Z. Cournia, and A. Klinakis, Magnetic nanoparticles coated with polyarabic acid demonstrate enhanced drug delivery and imaging properties for cancer theranostic applications, Sci. Rep. **7**, 775 (2017).
[31] R. A. Harris, H. van der Walt, and P. M. Shumbula, Molecular dynamics study on iron oxide nanoparticles stabilised with sebacic acid and 1,10-decanediol surfactants, J. Mol. Struct. **1048**, 18 (2013).
[32] R. A. Harris, P. M. Shumbula, and H. van der Walt, Analysis of the interaction of surfactants oleic acid and oleylamine with iron oxide nanoparticles through molecular mechanics modeling, Langmuir **31**, 3934 (2015).
[33] A. Hosseini nasr, H. Akbarzadeh, and R. Tayebee, Adsorption mechanism of different acyclovir concentrations on 1–2 nm sized magnetite nanoparticles: A molecular dynamics study, J. Mol. Liq. **254**, 64 (2018).
[34] M. Elstner, D. Porezag, G. Jungnickel, J. Elsner, M. Haugk, Th. Frauenheim, S. Suhai, and G. Seifert, Self-consistent-charge density-functional tight-binding method for simulations of complex materials properties, Phys. Rev. B **58**, 7260 (1998).
[35] A. V. Krukau, O. A. Vydrov, A. F. Izmaylov, and G. E. Scuseria, Influence of the exchange screening parameter on the performance of screened hybrid functionals, J. Chem. Phys. **125**, 224106 (2006).
[36] G. Zheng, H. A. Witek, P. Bobadova-Parvanova, S. Irle, D. G. Musaev, R. Prabhakar, and K. Morokuma, Parameter calibration of transition-metal elements for the spin-polarized self-consistent-charge density-functional tight-binding (DFTB) method: Sc, Ti, Fe, Co, and Ni, J. Chem. Theory Comput. **3**, 1349 (2007).
[37] R. Dovesi, R. Orlando, A. Erba, C. M. Zicovich-Wilson, B. Civalleri, S. Casassa, L. Maschio, M. Ferrabone, M. De La Pierre, P. D'Arco *et al.*, CRYSTAL14: A program for the ab initio investigation of crystalline solids, Int. J. Quantum Chem. **114**, 1287 (2014).
[38] R. Dovesi, V. R. Saunders, C. Roetti, R. Orlando, C. M. Zicovich-Wilson, F. Pascale, B. Civalleri, K. Doll, N. M. Harrison, I. J. Bush *et al.*, Crystal14 User's Manual (University of Torino, Torino, Italy, 2014).
[39] See Supplemental Material at http://link.aps.org/supplemental/10.1103/PhysRevLett.123.186101 for further computational details, numbers of different types of Fe ions in the nanoparticles, the relative total energy as a function of the total magnetic moment of the nanoparticles, the comparison between DFTB + U and HSE structures of the nanoparticles, the saturation magnetization of nanocubes of different sizes, the projected density of states of the nanoparticles, and charge density plots for some electronic states, which includes Refs. [40–44].
[40] G. Seifert and J. Joswig, Density-functional tight binding—An approximate density-functional theory method, Wiley Interdiscip. Rev.-Comput. Mol. Sci. **2**, 456 (2012).
[41] M. Elstner and G. Seifert, Density functional tight binding, Phil. Trans. R. Soc. A **372**, 20120483 (2014).
[42] B. Aradi, B. Hourahine, and T. Frauenheim, DFTB+, a sparse matrix-based implementation of the DFTB method, J. Phys. Chem. A **111**, 5678 (2007).
[43] B. Hourahine, S. Sanna, B. Aradi, C. Köhler, Th. Niehaus, and Th. Frauenheim, Self-interaction and strong correlation in DFTB, J. Phys. Chem. A **111**, 5671 (2007).
[44] H. C. Andersen, Molecular dynamics at constant pressure and/or temperature, J. Chem. Phys. **72**, 2384 (1980).
[45] H. Liu, G. Seifert, and C. Di Valentin, An efficient way to model complex magnetite: Assessment of SCC-DFTB against DFT, J. Chem. Phys. **150**, 094703 (2019).
[46] Y. Jun *et al.*, Nanoscale size effect of magnetic nanocrystals and their utilization for cancer diagnosis via magnetic resonance imaging, J. Am. Chem. Soc. **127**, 5732 (2005).
[47] D. Ling *et al.*, Multifunctional tumor ph-sensitive self-assembled nanoparticles for bimodal imaging and treatment of resistant heterogeneous tumors, J. Am. Chem. Soc. **136**, 5647 (2014).
[48] C. Prashant, Superparamagnetic iron oxide e Loaded poly (lactic acid)–D-a-tocopherol polyethylene glycol 1000 succinate copolymer nanoparticles as MRI contrast agent, Biomaterials **31**, 5588 (2010).
[49] D. Selli, G. Fazio, and C. Di Valentin, Modelling realistic TiO_2 nanospheres: A benchmark study of SCC-DFTB against hybrid DFT, J. Chem. Phys. **147**, 164701 (2017).
[50] J. P. Wright, J. P. Attfield, and P. G. Radaelli, Long Range Charge Ordering in Magnetite Below the Verwey Transition, Phys. Rev. Lett. **87**, 266401 (2001).

[51] I. Leonov, A. N. Yaresko, V. N. Antonov, M. A. Korotin, and V. I. Anisimov, Charge and Orbital Order in Fe_3O_4, Phys. Rev. Lett. **93**, 146404 (2004).

[52] H. T. Jeng, G. Y. Guo, and D. J. Huang, Charge-Orbital Ordering and Verwey Transition in Magnetite, Phys. Rev. Lett. **93**, 156403 (2004).

[53] J. Schlappa, C. Schüßler-Langeheine, C. F. Chang, H. Ott, A. Tanaka, Z. Hu, M. W. Haverkort, E. Schierle, E. Weschke, G. Kaindl, and L. H. Tjeng, Direct Observation of t_{2g} Orbital Ordering in Magnetite, Phys. Rev. Lett. **100**, 026406 (2008).

[54] S. C. Weng, Y. R. Lee, C. G. Chen, C. H. Chu, Y. L. Soo, and S. L. Chang, Direct Observation of Charge Ordering in Magnetite using Resonant Multiwave X-Ray Diffraction, Phys. Rev. Lett. **108**, 146404 (2012).

[55] M. S. Senn, J. P. Wright, and J. P. Attfield, Charge order and three-site distortions in the Verwey structure of magnetite, Nature (London) **481**, 173 (2012).

[56] Z. Nedelkoski, D. Kepaptsoglou, L. Lari, T. Wen, R. A. Booth *et al.*, Origin of reduced magnetization and domain formation in small magnetite nanoparticles, Sci. Rep. **7**, 45997 (2017).